Facile morphology-controllable synthesis and growth mechanism of ZnO nanostructures with excellent photocatalytic activity

Xiaofang Qin[1] · Honglan Cai[1] · Feng Wang[1] · Ping Yin[1] · Xiaofeng Zhang[1]

Abstract

ZnO nanostructures with different morphologies were prepared by a simple hydrothermal synthesis employing only $Zn(NO_3)_2 \cdot 6H_2O$ and NaOH as raw materials. The crystalline phase, morphology, and structures of ZnO nanomaterials were characterized by X-ray diffraction (XRD), scanning electron microscopy (SEM), and transmission electron microscopy (TEM). The results display that the particle-like, flower-like, and pencil-like ZnO nanostructures can be obtained by changing the amount of NaOH added for hydrothermal synthesis. The growth mechanism of different morphological ZnO products was obviously different, and the morphologies of ZnO transformed from particles and flowers to rods with the increase in the amount of added NaOH. The band gap (E_g) values of ZnO samples with different morphologies calculated using Kubelka–Munk formalism were 3.32, 3.29, 3.26 and 3.26 eV, respectively. The photoluminescence (PL) spectra exhibit that the different morphological ZnO nanostructures have four similar emission peaks at approximately 361, 384–389, 420, and 486 nm at room temperature. The photocatalytic performance of varying ZnO nanostructures was researched by degrading methylene blue (MB) under irradiation of UV light, and the degradation efficiency of all ZnO samples for MB reached more than 99% within 100 min.

Keywords ZnO · Nanostructures · Hydrothermal synthesis · Growth mechanism · Photocatalytic activity

1 Introduction

In recent years, the development of the printing and dyeing industry and the use of organic dyes have brought colors to our life. At the same time, refractory organic pollutants in industrial wastewater have caused severe pollution to soil and water resources, which not only destroy the natural environment, but also threaten human health [1–5]. To eliminate the environmental pollution caused by organic dye wastewater, various technologies and methods are formed and used in the treatment of organic dye wastewater [6–10]. Compared with traditional treatment technology, photocatalytic treatment is a very effective method to solve the problem of organic dye pollution with the advantages of environmental protection, economy, and high efficiency [11, 12].

As a typical n-type semiconductor material, zinc oxide (ZnO) is widely applied as catalyst support, adsorbent, photocatalyst, battery material, sensors, and so on, because of its width band gap (3.37 eV) and exciton binding energy (60 meV), high thermal conductivity, high electron mobility, and good thermal and chemical stability [13–19]. As everyone knows, the morphology and structure of materials have a very important impact on the optical, physical, chemical, and electrical properties, and their application. Therefore, to enhance various performances, many methods and means have been employed to synthesize and prepare ZnO materials with different morphologies and structures. For example, Pál et al. prepared flower-, prism- and raspberry-like ZnO particles via a template-free hydrothermal synthesis at different temperatures from 60 to 90℃ [20]. Zhang et al. obtained different ZnO nanostructures, including nanorods, nanoparticles, and mixtures of them, by changing the quality of NaOH and adding NaF in the process of hydrothermal synthesis [21]. Arellano-Cortaza et al. synthesized different morphological ZnO nanoparticles from a chemical process under the action of microwave and different pH values [22]. In addition, Lin et al. made use of $Zn(CH_3COO)_2 \cdot 2H_2O$,

✉ Feng Wang
  wf200818@126.com

✉ Xiaofeng Zhang
  ludongzxf@126.com

1 School of Chemistry and Materials Science, Ludong University, Yantai 264025, China

hexamethylenetetramine (HMTA), NaOH, and poly(vinyl pyrrolidone) (PVP) as sources to produce ZnO nanostructures with different morphologies, using a domestic microwave under 200 W power for 15 min [23]. Bao et al. utilized an ethylene glycol-assisted sonochemical method for synthesizing bouquet-like, twin sphere-like, and sphere-like ZnO nanostructures by controlling the alkaline medium, reaction pH and ultrasound time [24]. The above researches show that various methods and technologies can be used to realize the controlled synthesis of ZnO materials with different structures and morphologies by changing the experimental conditions. However, finding a simple, economical and effective method is still the focus of current research.

Herein, we only used $Zn(NO_3)_2·6H_2O$ and NaOH as raw materials to prepare ZnO nanomaterials through a simple hydrothermal method. The particle-like, flower-like and pencil-like ZnO nanostructures were obtained by controlling the amount of NaOH added for hydrothermal synthesis. The growth mechanism of ZnO nanostructures with different morphologies has been briefly discussed. The optical properties of ZnO nanostructures were measured by UV–Vis diffuse reflectance spectra (UV–Vis DRS) and PL spectra. The photocatalytic performance of ZnO nanomaterials with different morphologies was studied by the degradation of MB in simulant wastewater under the irradiation of UV light.

2 Experimental procedure

2.1 Materials and reagents

$Zn(NO_3)_2·6H_2O$ (zinc nitrate hexahydrate) and NaOH (sodium hydroxide) were bought from Tianjin Ruijinte Chemical Co., Ltd., China. Absolute ethanol (C_2H_5OH) was procured from Tianjin Aopusheng Chemical Co., Ltd., China. They were of analytical grade and were used directly without further purification. Deionized water used throughout the experiment was prepared by an ultrapure water system (UPH-1-40L, Ultrapure Technology Co., Ltd., Chengdu, China).

2.2 Synthesis of ZnO nanostructures

In a typical preparation process, 0.005 mol of $Zn(NO_3)_2·6H_2O$ was dissolved in 10 mL of deionized water in a beaker under magnetic stirring. In another beaker, 0.010 mol of NaOH was dissolved in deionized water of 10 mL. Then, the NaOH solution was slowly added to $Zn(NO_3)_2$ solution under stirring. After stirring for 0.5 h, the solution was transferred to a polytetrafluoroethylene-lined autoclave (25 mL) and kept at 120℃ for 24 h. After cooling to normal temperature, the white ZnO sample was obtained by centrifugal washing with deionized water and

absolute ethanol several times and drying at 80℃ for 12 h. Under the same other conditions, other ZnO samples were also produced by changing the amount of NaOH (0.015, 0.020, and 0.025 mol) added for hydrothermal synthesis. According to the amount of NaOH added in the preparation process, four ZnO samples are defined as ZnO-1, ZnO-2, ZnO-3, and ZnO-4.

2.3 Characterization

The chemical composition of the product was characterized by X-ray powder diffraction (XRD, Rigaku D/max2500VPC) using CuKα radiation ($\lambda = 0.15418$ nm). The morphology and structure of ZnO samples were measured by scanning electron microscope (SEM, JSM-5610LV) and transmission electron microscope (TEM, JEM-1230). UV–Vis diffuse reflectance spectra (UV–Vis DRS) of ZnO samples were recorded on a UV–Vis–NIR spectrometer (SolidSpec-3700, Shimadzu) using $BaSO_4$ as the background. The photoluminescence (PL) spectroscopy was measured by an LS-55 fluorescence spectrometer with an Xe lamp at room temperature.

2.4 Photocatalytic measurements

The photocatalytic properties of ZnO nanomaterials with different morphologies were studied by degrading MB in an aqueous solution under UV irradiation. In the experiment, 30 mg of ZnO samples was added to quartz tubes containing 50 mL of 10 mg/L MB solution. Before irradiation, they were kept away from light for 40 min in a multi-position photochemical reactor (CEL-LAB500E, Beijing Zhongjiao Jinyuan Technology Co., Ltd, China) to ensure the adsorption balance between ZnO and MB. Then, the photocatalytic degradation of MB was carried out under the irradiation of 350 W high-pressure Hg lamps (centered at 365 nm) for 100 min under magnetic stirring. During the degradation process, 3 mL of MB solution was taken every 20 min for centrifugation, and the absorbance test was conducted on a UNICO UV-7200 spectrophotometer at $\lambda_{max} = 664$ nm. The photocatalytic degradation efficiency was calculated by using the absorbance of MB at different times.

3 Results and discussion

X-ray diffraction (XRD) is the primary method to study the chemical composition and crystal phase of samples. XRD patterns of the samples obtained with different NaOH addition amounts in hydrothermal synthesis are shown in Fig. 1. It can be seen from XRD patterns that the four samples have the same diffraction peaks, which correspond to the characteristic diffraction peaks of hexagonal wurtzite ZnO structure. Some diffraction peaks at about 31.9°, 34.7°, 36.5°,
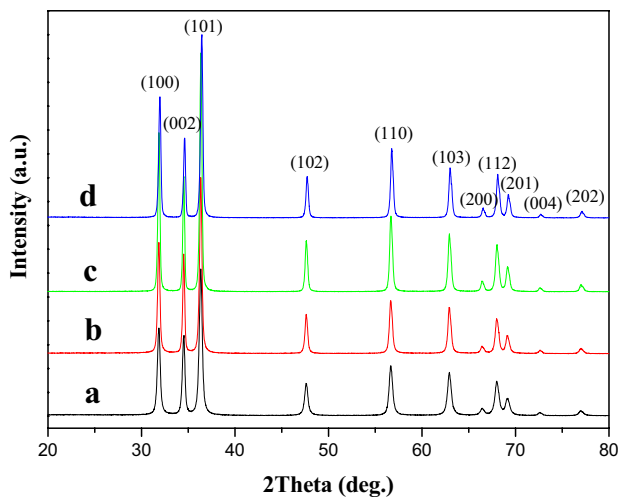
Fig. 1 XRD patterns of ZnO nanostructures obtained via hydrothermal synthesis with different amounts of added NaOH: **a** 0.010 mol; **b** 0.015 mol; **c** 0.020 mol; **d** 0.025 mol

**Table 1** The lattice constants (a, c) of ZnO samples with different morphologies

Samples		ZnO-1	ZnO-2	ZnO-3	ZnO-4
The lattice constants (Å)	a	3.24	3.23	3.22	3.22
	c	5.21	5.20	5.19	5.18

47.8°, 56.9°, 63.1° and 68.3° belong to the (100), (002), (101), (102), (110), (103) and (112) crystal planes of hexagonal ZnO [25–27]. The sharp and narrow diffraction peaks show that ZnO has a good crystal structure. According to the XRD data, the calculated lattice constants of four ZnO samples are shown in Table 1. As seen from Table 1, the lattice constants of the prepared ZnO samples are consistent with the standard value ($a = 3.25$ Å and $c = 5.21$ Å) of hexagonal ZnO lattice constant (JCPDS No. 36–1451) [25, 28]. No diffraction peaks of other substances were seen in the XRD, indicating that the obtained ZnO samples were of high purity. In addition, the intensity and width of the diffraction peak of ZnO do not change significantly with the amount of NaOH added in the preparation process. The XRD results show that the amount of NaOH added has no obvious effect on the crystalline phase of ZnO during the hydrothermal synthesis.

The morphology and structure of the ZnO samples were characterized by SEM and TEM. Figure 2 shows the SEM and TEM images of ZnO sample (ZnO-1) obtained on adding 0.010 mol of NaOH in hydrothermal synthesis. The SEM image (as shown in Fig. 2a) shows that the sample is mainly composed of particle-like ZnO. It can be clearly seen from the high magnification SEM image (Fig. 2b) that the shape and size of ZnO particles are irregular and inhomogeneous.

The TEM image (Fig. 2c) further exhibits that the ZnO sample has an irregular particle-like structure, and the size of the ZnO particles are between 100 and 500 nm. The TEM image of a typical irregular ZnO particle is shown in Fig. 2d. As shown in the TEM image, this particle consists of many smaller irregular nanoparticles with rough surface structure. The SEM and TEM images of ZnO-2 obtained by hydrothermal synthesis with 0.015 mol of NaOH are shown in Fig. 3. Figure 3a indicates the SEM image of the overall morphology of ZnO-2. It clearly shows that the obtained ZnO is composed of a large number of flower-like particle structures about 1–3 µm in size. The magnified SEM image of ZnO-2 in Fig. 3b reveals that the flower-like ZnO particles have a 3D hierarchical structure and are mainly composed of nanorods and a small amount of nanosheets. The diameter and length of nanorods are 50–100 nm and 500–800 nm, respectively, and the nanosheets have about 50–80 nm thickness. They are interspersed with each other in the particle to form a flower-like particle structure. The TEM image of ZnO-2 is proved in Fig. 3c, demonstrating that the sample has very well-defined flower-like ZnO particles with sharp raised surfaces. Figure 3d shows a TEM image of a typical flower-like ZnO particle with a size of about 2.3 µm. The surface of the ZnO flower has a tip protrusion structure, completely different from the surface structure (rough surface structure) of ZnO-1 (see Fig. 2d). This may be caused by the further growth of rough surface particles under the action of excess NaOH.
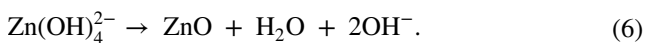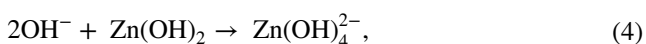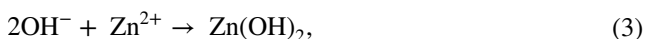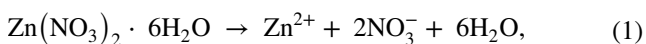
Figure 4 shows the SEM and TEM images of ZnO-3 and ZnO-4 obtained via hydrothermal synthesis with 0.020 mol and 0.025 mol NaOH, respectively. The low-magnification SEM image of ZnO-3 is shown in Fig. 4a. It can be seen from SEM image that the morphology of ZnO-3 is uniformity with high yield. The high-magnification SEM images (Fig. 4b) of ZnO-3 further show that it is composed of a large number of rods with a pencil-like structure, and the length and diameter of pencil-like ZnO rods are 1–2 µm and 100–250 nm, respectively. Figure 4c shows the TEM image of ZnO-3, indicating pencil-like ZnO rods. The TEM image (Fig. 4d) of a typical ZnO rod confirms the pencil-like structure with about 120 nm and 1.6 µm diameter and length. From the SEM and TEM images (Figs. 2, 3 and 4) of ZnO-1, ZnO-2 and ZnO-3, it can be found that the amount of NaOH added has an important effect on the morphology and structure of ZnO samples. With the increase in the addition amount of NaOH in hydrothermal synthesis, the morphology of ZnO samples changes from particle-like and flower-like to pencil-like structures. Figure 4e shows the TEM image of ZnO-4 obtained by hydrothermal synthesis with 0.025 mol NaOH. As clearly seen from the TEM image, the morphology of the ZnO-4 sample is still regular and has a uniform pencil-like structure. The TEM image (Fig. 4f) of a complete pencil-like ZnO rod shows that the diameter and length are about 150 nm and 2 µm, respectively.
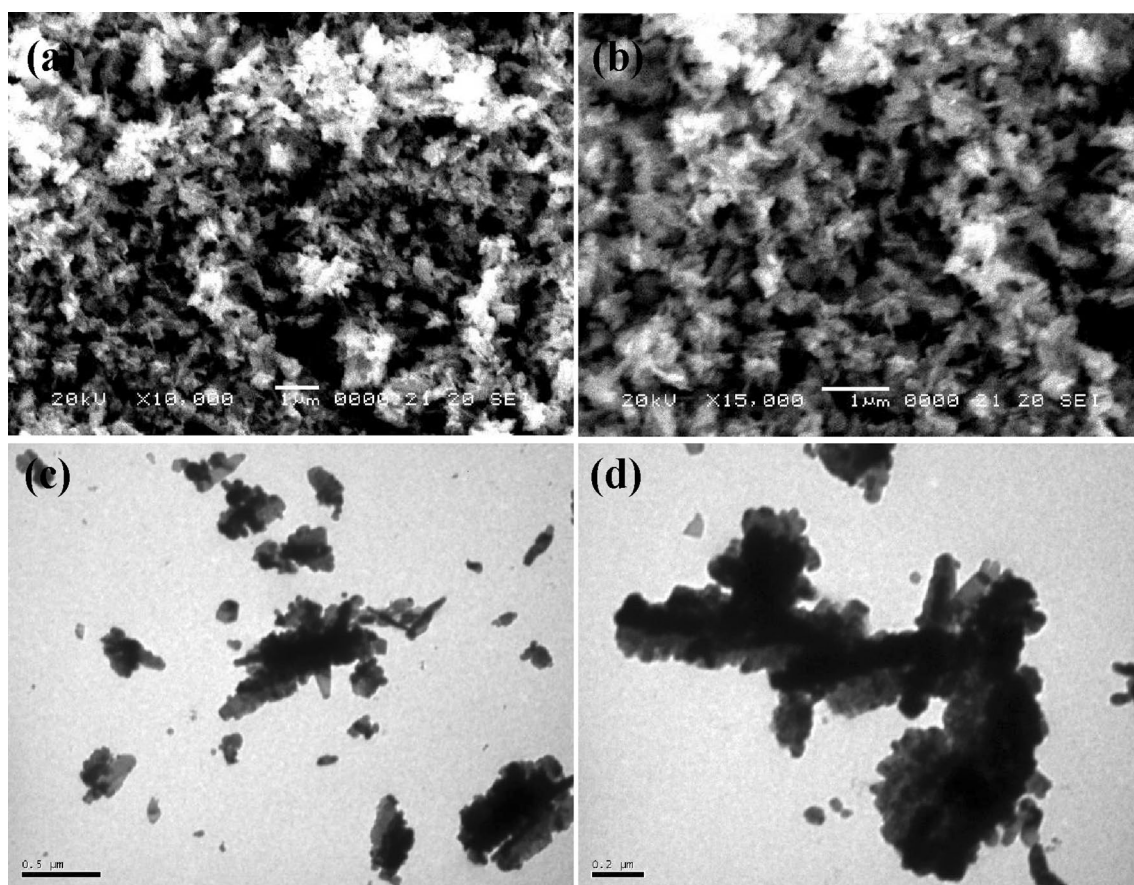
Fig. 2 SEM (**a**, **b**) and TEM (**c**, **d**) images of particle-like ZnO sample (ZnO-1)

These results show that the morphology and structure of ZnO do not change significantly when the amount of NaOH added is further increased in hydrothermal synthesis.

To study the growth mechanism of ZnO nanostructures with different morphologies, the possible chemical reaction process throughout the experiment can be described as follows [16, 29–31]:

$$Zn(NO_3)_2 \cdot 6H_2O \rightarrow Zn^{2+} + 2NO_3^- + 6H_2O, \tag{1}$$

$$NaOH \rightarrow OH^- + Na^+, \tag{2}$$

$$2OH^- + Zn^{2+} \rightarrow Zn(OH)_2, \tag{3}$$

$$2OH^- + Zn(OH)_2 \rightarrow Zn(OH)_4^{2-}, \tag{4}$$

$$Zn(OH)_2 \rightarrow ZnO + H_2O, \tag{5}$$

$$Zn(OH)_4^{2-} \rightarrow ZnO + H_2O + 2OH^-. \tag{6}$$

The above equations show that the content of OH^- ion plays a very important role in the chemical reaction and the formation and crystal growth of ZnO nuclei. According to the present experimental results (SEM and TEM results) and analysis, the reasonable growth process of ZnO nanostructures with different morphologies is shown in Fig. 5. When $Zn(NO_3)_2 \cdot 6H_2O$ and NaOH were dissolved in deionized water, Zn^{2+} ions and OH^- ions were obtained through Eq. (1) and Eq. (2), respectively. Then, when NaOH solution was added to $Zn(NO_3)_2$ solution, different precursors of ZnO nuclei are formed with different contents of NaOH in NaOH solution. The growth modes of ZnO nanostructures with different morphologies might relate to ZnO nuclei formed from different precursors. When the molar ratio of OH^- to Zn^{2+} is 2:1 (0.010 molar OH^-, 0.005 molar Zn^{2+}) in solution, the $Zn(OH)_2$ precursors were synthesized as in Eq. (3) with the stoichiometric ratio. In the initial stage of hydrothermal synthesis, many ZnO nuclei (represented by black dots ●) are formed through the thermal decomposition of $Zn(OH)_2$ precursors [as shown in Eq. (4)] at 120°. With the extension of hydrothermal synthesis time (24 h), particle-like ZnO nanostructures were obtained through the crystal nucleus growth and particles agglomeration in a neutral environment (pH 7). When the molar ratio of OH^- to
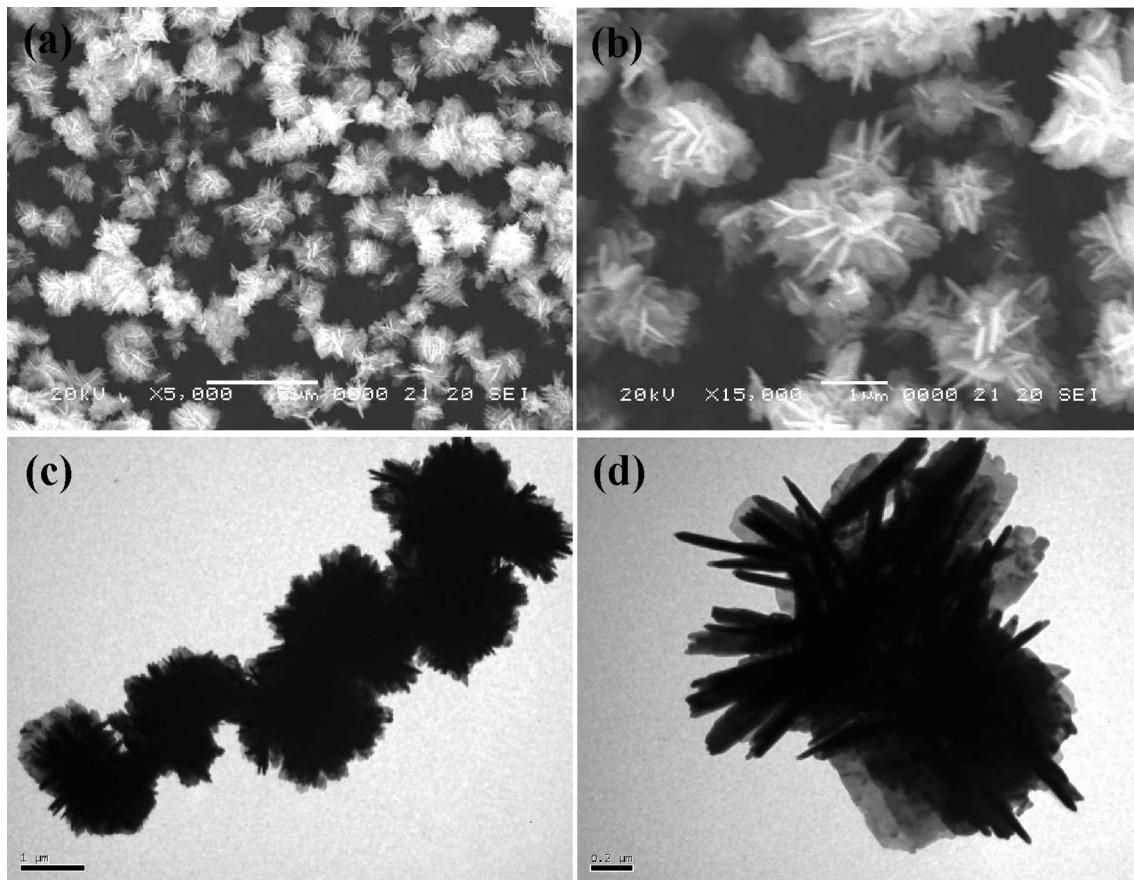
Fig. 3 SEM (**a**, **b**) and TEM (**c**, **d**) images of flower-like ZnO sample (ZnO-2)

Zn^{2+} increases to 3:1 (0.015 molar OH^-, 0.005 molar Zn^{2+}), the $Zn(OH)_2$ and $Zn(OH)_4^{2-}$ precursors were generated via Eq. (3) and Eq. (4). At hydrothermal synthesis temperature (120°), two kinds of ZnO nuclei with different surface structures and properties (marked with black dots ● and red dots ●) were produced from the thermal decomposition of different precursors ($Zn(OH)_2$ and $Zn(OH)_4^{2-}$) as shown in Eq. (5) and Eq. (6), respectively. At the same time, OH^- ions are also generated as shown in Eq. (6), which makes the hydrothermal synthesis environment strong alkaline (pH > 13). Then, the crystal nuclei from $Zn(OH)_2$ precursor grow into ZnO particles with the reaction time. In the meantime, other ZnO nuclei from the $Zn(OH)_4^{2-}$ precursor (marked with red dots ●) with OH^- ions adsorbed on the surface grow into pencil-like ZnO rods in the particles along the C-axis direction in a strong alkaline environment [32, 33]. During the growth of ZnO particles and rods, they are interspersed with each other to form a flower-like ZnO structure, as shown in Fig. 3. When the molar ratio of OH^- to Zn^{2+} is further expanded to 4:1 and 5:1 (0.020 and 0.025 molar OH^-, 0.005 molar Zn^{2+}), only $Zn(OH)_4^{2-}$ precursors were obtained via the reactions in Eq. (3) and Eq. (4) at room temperature. At 120°, the ZnO nuclei (marked with red dots ●) were produced from $Zn(OH)_4^{2-}$ precursor by Eq. (6),

and OH^- ions were also obtained. In an alkaline environment (pH > 13), pencil-like ZnO rods were prepared from the crystal growth of the ZnO nuclei at the C-axis direction with the extension of the time of hydrothermal synthesis [32, 33]. In short, the amount of NaOH added has an important effect on the structure of ZnO in the present experiments, and the morphology of ZnO nanostructures changes significantly from particles and flowers to rods with the increase of molar ratio of OH^- to Zn^{2+} in the hydrothermal synthesis.

The optical energy band gap (E_g) of ZnO nanostructures was studied by UV–Vis diffuse reflectance spectra. Figure 6 shows the UV–Vis diffuse reflectance spectra of all the ZnO samples with different morphologies at room temperature from 300 to 800 nm. From Fig. 6, it can be found that all the ZnO samples have strong reflection above 400 nm, which is consistent with previous reports [34]. The E_g of the prepared ZnO samples can be calculated according to Kubelka–Munk (K–M) function using the following equations [34–36]:

$$F(R) = (1 - R)^2/2R, \tag{7}$$

$$(F(R)h\nu)^2 = B(h\nu - E_g), \tag{8}$$
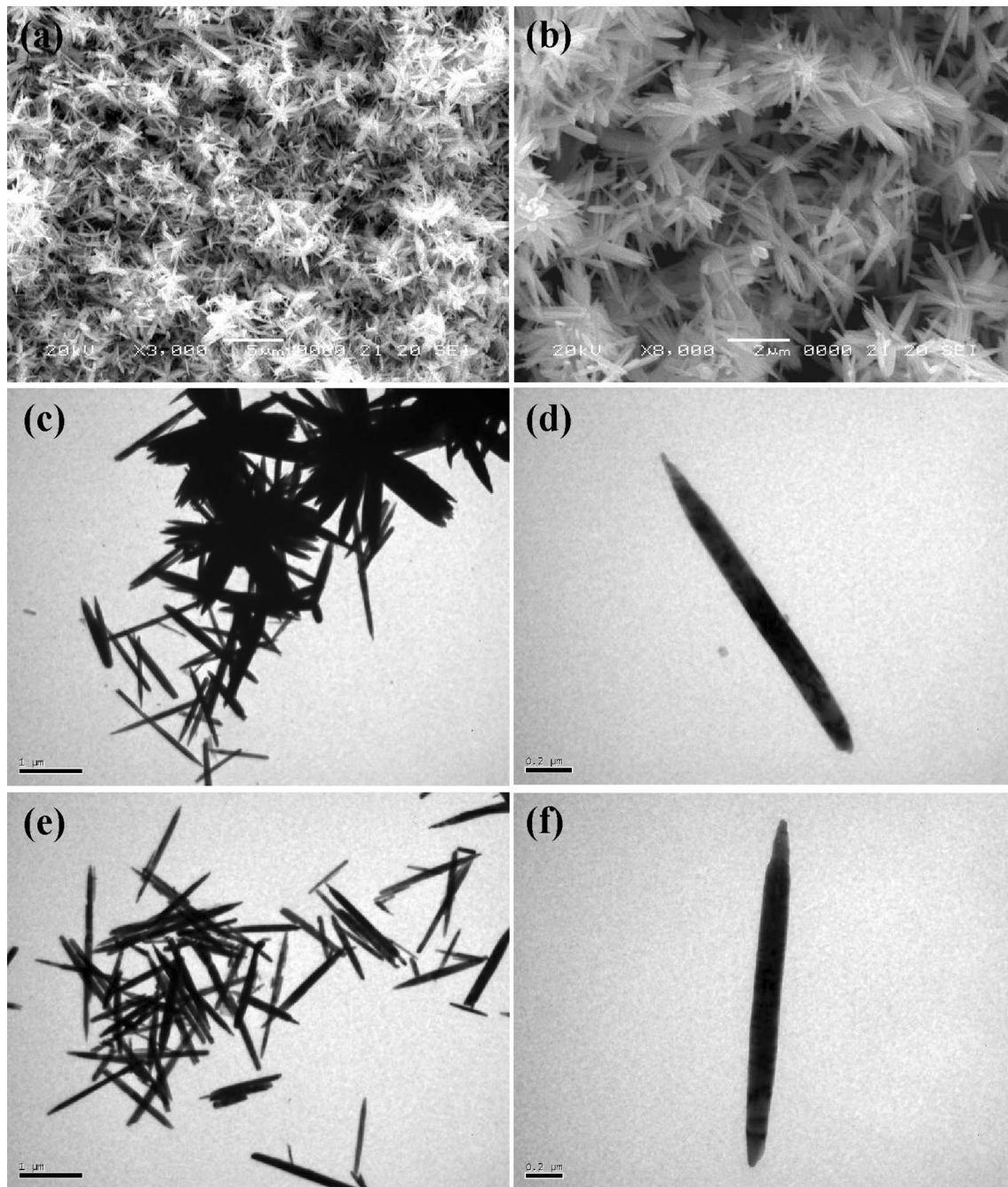
Fig. 4 SEM (**a**, **b**) and TEM (**c**, **d**) images of pencil-like ZnO sample (ZnO-3), and TEM (**e**, **f**) images of pencil-like ZnO sample (ZnO-4)

where $F(R)$ is the Kubelka–Munk function, R is the reflectance of the sample, E_g is the band gap energy of the sample, $h\nu$ is the photon energy and B is a proportionality constant. Figure 7 shows the plot of $[F(R)h\nu]^2$ versus photon energy of all the ZnO samples. The E_g values of all the ZnO samples calculated by diffuse reflectance using Kubelka–Munk formalism is shown in Table 2. As seen in Table 2, the E_g values of ZnO samples with different morphologies were 3.32,

3.29, 3.26 and 3.26, respectively. The E_g of ZnO samples has an obvious decrease with the morphology changes from nanoparticles to nanorods. In addition, the E_g of all the ZnO nanostructures has also an obvious decrease compared with that of the bulk ZnO sample ($E_g = 3.37$ eV). The decrease of E_g may be related to the quantum confinement effect, crystal defect structure and material morphology.

The PL property of the different morphological ZnO samples was carried out with a 325 nm of excitation wavelength.

Fig. 5 Schematic illustration of the formation mechanism of ZnO nanostructures with different morphologies
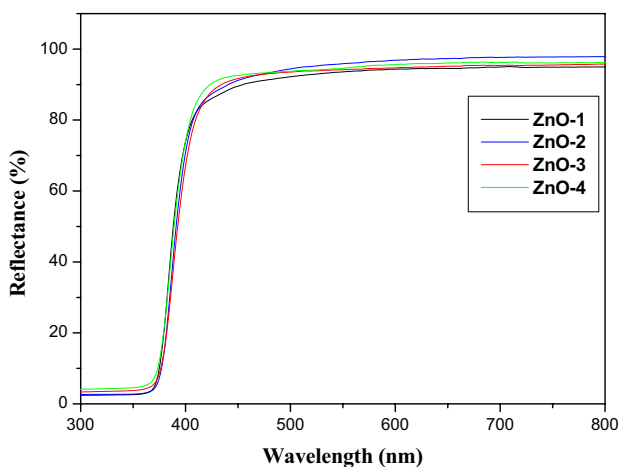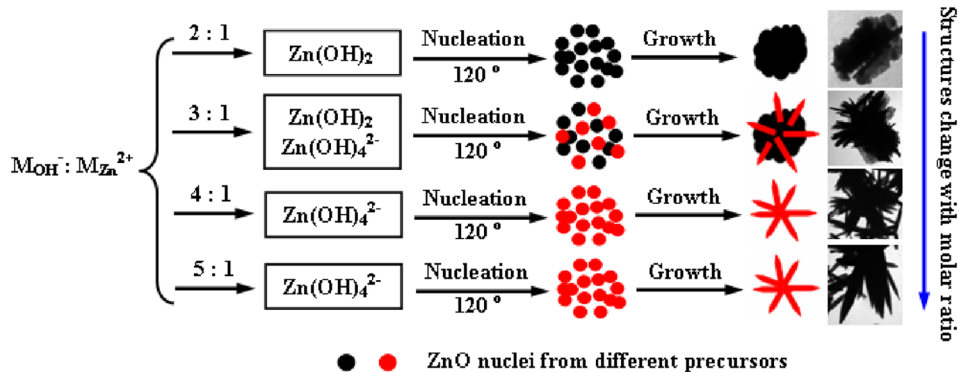
Fig. 6 UV–Vis diffuse reflectance spectra of ZnO samples with different morphologies at room temperature

The PL spectra of the four ZnO samples are shown in Fig. 8. It can be clearly found from PL spectra that all ZnO samples exhibit four similar emission peaks marked at about 361, 384–389, 420 and 486 nm. The two ultraviolet (UV) peaks at about 361 and 384 (or 389, 389, and 386) nm are related to the near band edge emission of ZnO materials, which is due to the direct recombination of conduction band electrons and valence band holes [37, 38]. In addition, compared with the emission peak of particle-like ZnO nanostructures at 384 nm and that of flower-like and pencil-like ZnO nanostructures also have a red-shift of 5–2 nm (at 389 and 386 nm). This may be due to the different morphology, structure and particle sizes of ZnO samples. The weak emission peaks at 420 and 486 nm may be attributed to the transition from the ionized charged oxygen vacancy level to the valence band [39, 40]. The UV–Vis and PL spectra prove that the prepared ZnO nanomaterials have excellent optical properties. Therefore, they can be widely used in the field of photocatalysis as photocatalysts.

It is well known that the morphology, structure and specific surface area have important effects on the photocatalytic performance of the materials [41, 42]. Methylene blue (MB) solution was used to simulate organic dye wastewater to study the photocatalytic performance of the prepared ZnO nanostructures with different morphologies. Figure 9 exhibits the photocatalytic efficiency curves of ZnO with different morphologies for photocatalytic degradation of MB in an aqueous solution under UV irradiation. The black dotted line on the left side of the figure indicates the time required for the ZnO sample to adsorb MB to reach equilibrium, and the maximum adsorption efficiency of four ZnO samples for MB was about 17.4% after 40 min. This shows that the adsorption capacity of ZnO samples for MB is not significant. The photocatalytic results showed that only a small amount of MB (about 17.2%) was degraded under UV irradiation after 100 min without photocatalyst, as shown in Fig. 9a. In contrast, the degradation rates of MB were obviously improved when ZnO samples were used as photocatalysts in the MB aqueous solution. From Fig. 9b–e, it can be seen that the degradation rates of MB by ZnO samples with different morphology and structure are more than 99% within 60 min, and the maximum degradation rate of flower-like ZnO nanostructure can reach 99.5% (Fig. 9c) after 100 min of UV irradiation. The results of the photocatalytic experiment show that the prepared ZnO samples have very high photocatalytic degradation efficiency for MB. The mechanism of photocatalytic degradation of organic dyes by ZnO catalysts is described as follows. The electrons on the valence band (VB) are excited to the conduction band (CB) to form electron–hole pairs ($e^−$–h^+) when the light shines on the surface of ZnO nanomaterials [Eq. (9)]. The holes (h^+) have strong oxidation and can oxidize hydroxyl ions ($OH^−$) and water molecules (H_2O) adsorbed on the surface of ZnO nanomaterials into strong oxidants—hydroxyl radicals ($OH·$) [Eq. (10) and (11)]. The excited electrons ($e^−$) in the CB react with oxygen (O_2) adsorbed on the ZnO surface and form superoxide radicals ($O_2^−·$) [Eq. (12)]. Then, they ($OH·$ and $O_2^−$) degrade the organic dye molecules (MB) on the surface of ZnO photocatalysts into harmless compounds, such as carbon dioxide (CO_2) and water (H_2O) [Eq. (13) and (14)] [41, 43, 44].
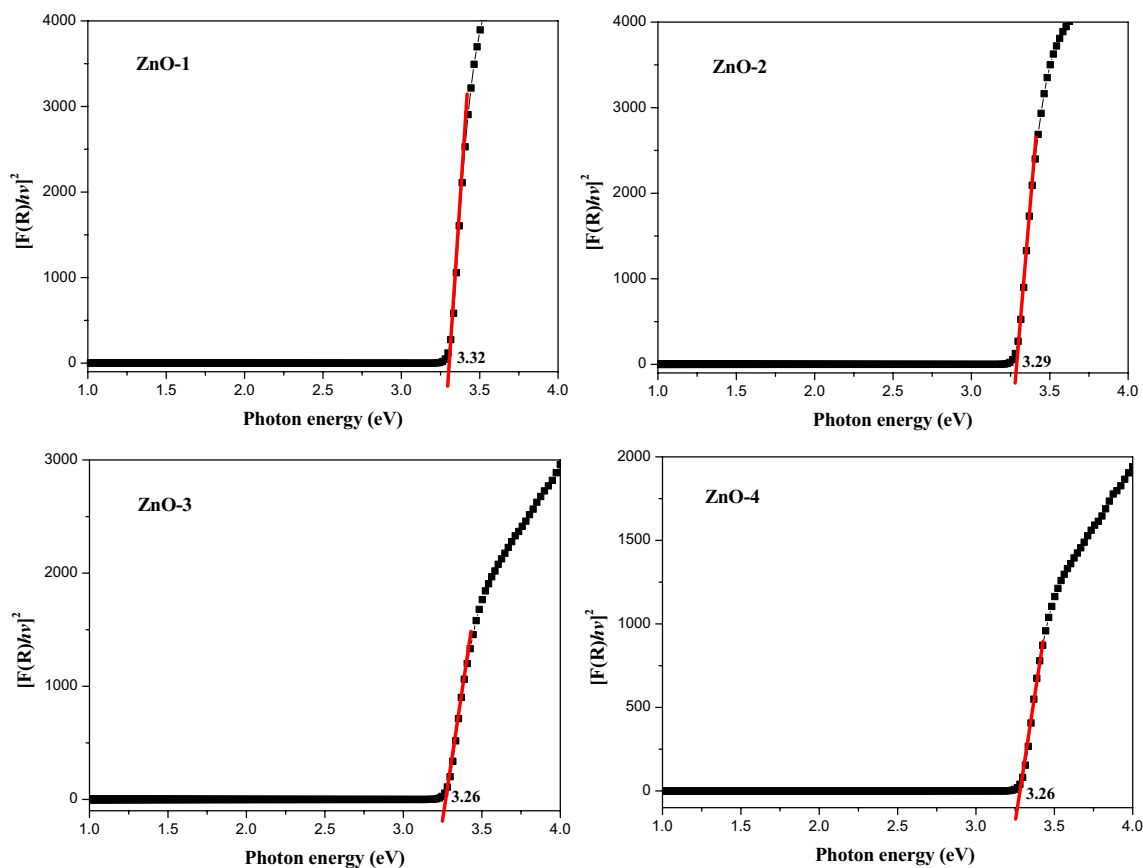
Fig. 7 Kubelka–Munk function versus photon energy plots of all the ZnO samples

Table 2 The optical band gap (E_g) of ZnO samples calculated by diffuse reflectance using the Kubelka–Munk formalism

Samples	ZnO-1	ZnO-2	ZnO-3	ZnO-4
Band gap energy, E_g (eV)	3.32	3.29	3.26	3.26

$$ZnO + h\nu \rightarrow ZnO\left(e^- + h^+\right), \tag{9}$$

$$h^+ + H_2O \rightarrow OH\cdot + H^+, \tag{10}$$

$$h^+ + OH^- \rightarrow OH\cdot, \tag{11}$$

$$2e^- + O_2 \rightarrow O_2^-\cdot, \tag{12}$$

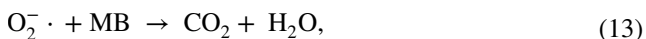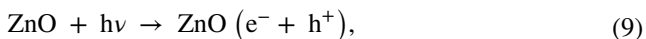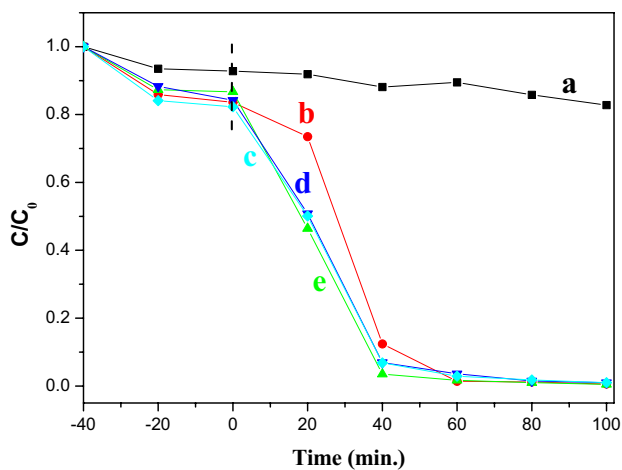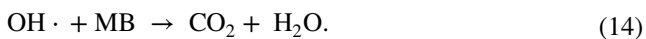$$O_2^-\cdot + MB \rightarrow CO_2 + H_2O, \tag{13}$$
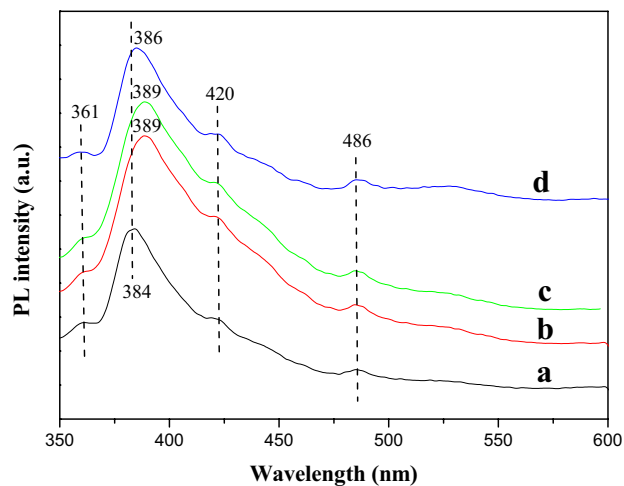
Fig. 8 Photoluminescence spectra of ZnO nanostructures with different morphologies at room temperature

Fig. 9 Photocatalytic degradation curves of methylene blue (MB) under UV light **a** without catalysts, **b** with particle-like ZnO, **c** with flower-like ZnO, and **d**, **e** with pencil-like ZnO nanorods

$$OH \cdot + MB \ \rightarrow \ CO_2 + \ H_2O. \tag{14}$$

At the same time, we also compared the photocatalytic performance of ZnO nanomaterials for MB obtained in this experiment with that of ZnO nanomaterials obtained by other technologies, as shown in Table 3. As can be seen from Table 3, all the ZnO samples with different morphologies obtained in this work showed better photocatalytic activity as compared to that of the literature. Therefore, the prepared ZnO nanostructures with different morphologies can be widely used to treat the organic dye wastewater by photocatalytic degradation and show excellent photocatalytic performance.

4 Conclusions

The particle-like, flower-like, and pencil-like ZnO nanostructures were fabricated by controlling the amount of NaOH added for hydrothermal synthesis. With the increase of the amount of NaOH, the growth process of ZnO nanostructures with different morphologies is obviously different from particles, flowers or rods. The E_g of ZnO samples calculated by UV–Vis diffuse reflectance using Kubelka–Munk formalism has an obvious decrease from 3.32 to 3.26 eV with the morphology changes from nanoparticles to nanorods. The ZnO samples have similar PL emission peaks at about 361, 384–389, 420 and 486 nm at room temperature. The prepared ZnO nanomaterials show excellent photocatalytic degradation efficiency for methylene blue, and the maximum degradation efficiency can reach 99.5% within 100 min.

Table 3 The comparison of the photocatalytic performance of ZnO nanomaterials obtained by different technologies

Synthesis method	Sample morphology	UV irradiation time (min)	Degradation rate (%)	References
Microwave irradiation	Spherical nanostructures	240	78%	[43]
Hydrothermal synthesis	Nanoplate clusters	60	99.7%	[45]
	Nanorods	60	63%	
Hydrothermal synthesis	Nanorods	120	12.3%	[46]
	Nanoparticles	120	25.2%	
Sol–gel method	Nanoparticles	210	92.7%	[41]
Coprecipitation	Nanoparticles	360	79%	[47]
Green synthesis	Nanoparticles	210	98.6%	[48]
Solvothermal approach	Polyprisms	50	94.1%	[49]
	Spindle-shape structures	50	69.6%	
Spray pyrolysis	Thin films	120	82.1%	[50]
Hydrothermal synthesis	Nanoflowers	100	99.5%	This work
	Nanorods	100	99.1%	
	Nanoparticles	100	99.4%	

Data availability All data generated or analysed during this study are included in this published article.

Declarations

Conflict of interest The authors declare no conflict of interest.

References

1. K.M. Lee, C.W. Lai, K.S. Ngai, J.C. Juan, Recent developments of zinc oxide based photocatalyst in water treatment technology: a review. Water Res. **88**, 428–448 (2016)
2. S. Sangon, A.J. Hunt, T.M. Attard, P. Mengchang, Y. Ngernyen, N. Supanchaiyamat, Valorisation of waste rice straw for the production of highly effective carbon based adsorbents for dyes removal. J. Clean. Prod. **172**, 1128–1139 (2018)
3. M. Jain, S.A. Khan, K. Sharma, P.R. Jadhao, K.K. Pant, Z.M. Ziora, M.A.T. Blaskovich, Current perspective of innovative strategies for bioremediation of organic pollutants from wastewater. Bioresour. Technol. **344**, 126305 (2022)
4. Q. Zhou, Chemical pollution and transport of organic dyes in water–soil–crop systems of the Chinese coast. Bull. Environ. Contam. Tox. **66**, 784–793 (2001)
5. K. He, G.Q. Chen, G.M. Zeng, A.W. Chen, Z.Z. Huang, J.B. Shi, T.T. Huang, M. Peng, L. Hu, Three-dimensional graphene supported catalysts for organic dyes degradation. Appl. Catal. B Environ. **228**, 19–28 (2018)
6. W. Zhao, W. Chen, F.Q. Huang, Toward large-scale water treatment using nanomaterials. Nano Today **27**, 11–27 (2019)
7. Y.Y. An, H.L. Zheng, Q. Sun, X.Y. Zheng, W.Q. Liu, X.M. Tang, Z.K. Xiong, Two-step synthesis of a single-layer grafting self-floating adsorbent for anionic dyes adsorption, surface separation and concentration. J. Hazard. Mater. **384**, 121262 (2020)
8. D. González-Muñoz, A. Gómez-Avilés, C.B. Molina, J. Bedia, C. Belver, J. Alemán, S. Cabrera, Anchoring of 10-phenylphenothiazine to mesoporous silica materials: a water compatible organic photocatalyst for the degradation of pollutants. J. Mater. Sci. Technol. **103**, 134–143 (2022)
9. G.D. Jimenez, T. Monti, J.J. Titman, V. Hernandez-Montoya, S.W. Kingman, E.R. Binner, New insights into microwave pyrolysis of biomass: preparation of carbon-based products from pecan nutshells and their application in wastewater treatment. J. Anal. Appl. Pyrol. **124**, 113–121 (2017)
10. A.P. Zhang, Z.P. Gu, W.M. Chen, Q.B. Li, G.B. Jiang, Removal of refractory organic pollutants in reverse-osmosis concentrated leachate by microwave-Fenton process. Environ. Sci. Pollut. Res. **25**, 28907–28916 (2018)
11. M. Samadi, M. Zirak, A. Naseri, M. Kheirabadi, M. Ebrahimi, A.Z. Moshfegh, Design and tailoring of one-dimensional ZnO nanomaterials for photocatalytic degradation of organic dyes: a review. Res. Chem. Intermediat. **45**, 2197–2254 (2019)
12. A. Ajmal, I. Majeed, R.N. Malik, M. Iqbal, M. Arif Nadeem, I. Hussain, S. Yousaf, G. Zeshan, G. Mustafa, M.I. Zafar, M.A. Nadeem, Photocatalytic degradation of textile dyes on Cu_2O-CuO/TiO_2 anatase powders. J. Environ. Chem. Eng. **4**, 2138–2146 (2016)
13. D.Z. Zhang, Y.E. Sun, C.X. Jiang, Y. Yao, D.Y. Wang, Y. Zhang, Room-temperature highly sensitive CO gas sensor based on Ag-loaded zinc oxide/molybdenum disulfide ternary nanocomposite
    and its sensing properties. Sensor. Actuat. B Chem. **253**, 1120–1128 (2017)
14. M.H. Kahsay, A. Tadesse, D. RamaDevi, N. Belachew, K. Basavaiah, Green synthesis of zinc oxide nanostructures and investigation of their photocatalytic and bactericidal applications. RSC Adv. **9**, 36967–36981 (2019)
15. A.H. Javed, N. Shahzad, M.A. Khan, M. Ayub, N. Iqbal, M. Hassan, N. Hussain, M.I. Rameel, M.I. Shahzad, Effect of ZnO nanostructures on the performance of dye sensitized solar cells. Sol. Energy **230**, 492–500 (2021)
16. C. Peng, J.J. Guo, W.K. Yang, C.K. Shi, M.R. Liu, Y.X. Zheng, J. Xu, P.Q. Chen, T.T. Huang, Y.Q. Yang, Synthesis of three-dimensional flower-like hierarchical ZnO nanostructure and its enhanced acetone gas sensing properties. J. Alloy. Compd. **654**, 371–378 (2016)
17. M.H. Liu, Y.W. Chen, T.S. Lin, C.Y. Mou, Defective mesocrystal ZnO-supported gold catalysts: facilitating CO oxidation via vacancy defects in ZnO. ACS Catal. **8**, 6862–6869 (2018)
18. M.L. Huang, J.D. Lin, R. Li, Y.H. Su, X.J. Zhao, Y.B. Liu, W.J. Chen, X.B. Lian, X.X. Chen, X.Y. Pan, Hierarchical ZnO nanosheet-reduced graphene oxide composites for photocatalytic ethylene oxidation. ACS Appl. Nano Mater. **5**, 1828–1835 (2022)
19. D.Z. Zhang, W.J. Pan, L.J. Zhou, S.J. Yu, Room-temperature benzene sensing with Au-doped ZnO nanorods/exfoliated WSe_2 nanosheets and density functional theory simulations. ACS Appl. Mater. Inter. **13**, 33392–33403 (2021)
20. E. Pál, V. Hornok, R. Kun, V. Chernyshev, T. Seemann, I. Dékány, M. Busse, Growth of raspberry-, prism- and flower-like ZnO particles using template-free low-temperature hydrothermal method and their application as humidity sensors. J. Nanopart. Res. **14**, 1002 (2012)
21. J.P. Zhang, T.M. Liu, Y. Zhang, W. Zeng, F.S. Pan, X.H. Peng, Hydrothermal synthesis and growth mechanisms of different ZnO nanostructures and their gas-sensing properties. J. Mater. Sci. Mater. Electron. **26**, 1347–1353 (2015)
22. M. Arellano-Cortaza, E. Ramírez-Morales, U. Pal, G. Pérez-Hernández, L. Rojas-Blanco, pH dependent morphology and texture evolution of ZnO nanoparticles fabricated by microwave-assisted chemical synthesis and their photocatalytic dye degradation activities. Ceram. Inter. **47**, 27469–27478 (2021)
23. S. El-Nahas, M.S. Abd El-sadek, H.M. Salman, M.M. Elkady, Controlled morphological and physical properties of ZnO nanostructures synthesized by domestic microwave route. Mater. Chem. Phys. **258**, 123885 (2021)
24. Y. Bao, L. Gao, C.P. Feng, J.Z. Ma, S. Lyu, Systematically controlled synthesis of shape-selective ZnO superstructures via sonochemical process. Mater. Sci. Eng. B **263**, 114887 (2021)
25. F. Wang, X.F. Qin, Z.L. Guo, Y.F. Meng, L.X. Yang, Y.F. Ming, Hydrothermal synthesis of dumbbell-shaped ZnO microstructures. Ceram. Inter. **39**, 8969–8973 (2013)
26. P. Rai, W.K. Kwak, Y.T. Yu, Solvothermal synthesis of ZnO nanostructures and their morphology-dependent gas-sensing properties. ACS Appl. Mater. Inter. **5**, 3026–3032 (2013)
27. D.Z. Zhang, J.F. Wu, P. Li, Y.H. Cao, Z.M. Yang, Hierarchical nanoheterostructure of tungsten disulfide nanoflowers doped with zinc oxide hollow spheres: benzene gas sensing properties and first-principles study. ACS Appl. Mater. Inter. **11**, 31245–31256 (2019)
28. J.D. Li, H.J. Zhao, M.M. Wang, Y.Y. Zhu, B. Li, X.Q. Yu, J.C. Xu, Y.J. Cheng, L.Z. Ouyang, H.Y. Shao, Rational design of 3D N-doped carbon nanosheet framework encapsulated ultrafine ZnO nanocrystals as superior performance anode materials in lithium ion batteries. J. Mater. Chem. A **7**, 25155–25164 (2019)
29. C.C. Lin, Y.C. You, Mass-production of ZnO nanoparticles by precipitation in a rotating packed bed: effect of zinc salt. J. Mater. Res. Technol. **9**, 8451–8458 (2020)

30. L. Zhu, Y. Li, W. Zeng, Hydrothermal synthesis of hierarchical flower-like ZnO nanostructure and its enhanced ethanol gas-sensing properties. Appl. Surf. Sci. **427**, 281–287 (2018)

31. K. Pal, T.P. Majumder, S.C. Debnath, S. Ghosh, S.K. Roy, Self-enhanced controllable growth of ZnO micro-flowers from nano-spikes and its transformation to nanoparticles by using compositional variation: essential dielectric switching applications. J. Mol. Struct. **1027**, 36–43 (2012)

32. H.Q. Wang, C.H. Li, H.G. Zhao, J.R. Liu, Preparation of nanosized flower-like ZnO bunches by a direct precipitation method. Adv. Powder Technol. **24**, 599–604 (2013)

33. L. Sun, R. Shao, Z.D. Chen, L.Q. Tang, Y. Dai, J.F. Ding, Alkali-dependent synthesis of flower-like ZnO structures with enhanced photocatalytic activity via a facile hydrothermal method. Appl. Sur. Sci. **258**, 5455–5461 (2012)

34. L.K. Jangir, Y. Kumari, A. Kumar, M. Kumar, K. Awasthi, Investigation of luminescence and structural properties of ZnO nanoparticles, synthesized with different precursors. Mater. Chem. Front. **1**, 1413–1421 (2017)

35. M.A. Ciciliati, M.F. Silva, D.M. Fernandes, M.A.C. de Melo, A.A.W. Hechenleitner, E.A.G. Pineda, Fe-doped ZnO nanoparticles: Synthesis by a modified sol-gel method and characterization. Mater. Lett. **159**, 84–86 (2015)

36. R.O. Yathisha, Y.A. Nayaka, Effect of solvents on structural, optical and electrical properties of ZnO nanoparticles synthesized by microwave heating route. Inorg. Chem. Commun. **115**, 107877 (2020)

37. V. Srikant, D.R. Clarke, On the optical band gap of zinc oxide. J. Appl. Phys. **83**, 5447–5451 (1998)

38. L.B. Wang, Y.P. Fan, H. Bala, G. Sun, Controllable synthesis of hierarchical ZnO microstructures via a hydrothermal route, Micro. Nano Lett. **6**, 741–744 (2011)

39. J.S. Liu, J.M. Cao, Z.Q. Li, G.B. Ji, M.B. Zheng, A simple microwave-assisted decomposing route for synthesis of ZnO nanorods in the presence of PEG400. Mater. Lett. **61**, 4409–4411 (2007)

40. L.Q. Tang, Y.M. Tian, Y.H. Liu, Z.C. Wang, B. Zhou, One-step solution synthesis of urchin-like ZnO superstructures from ZnO rods. Ceram. Inter. **39**, 2303–2308 (2013)

41. S. Demirci, T. Dikici, M.M. Tünçay, N. Kaya, A study of heating rate effect on the photocatalytic performances of ZnO powders prepared by sol-gel route: their kinetic and thermodynamic studies. Appl. Surf. Sci. **507**, 145083 (2020)

42. H.P. Lia, J.X. Liu, C. Wang, H. Yang, X.X. Xue, Oxygen vacancies-enriched and porous hierarchical structures of ZnO microspheres with improved photocatalytic performance. Vacuum **199**, 110891 (2022)

43. A. Kajbafvala, H. Ghorbani, A. Paravar, J.P. Samberg, E. Kajbafvala, S.K. Sadrnezhaad, Effects of morphology on photocatalytic performance of zinc oxide nanostructures synthesized by rapid microwave irradiation methods. Superlattice. Microst. **51**, 512–522 (2012)

44. T.S. Aldeen, H.E.A. Mohamed, M. Maaza, ZnO nanoparticles prepared via a green synthesis approach: physical properties, photocatalytic and antibacterial activity. J. Phys. Chem. Solids **160**, 110313 (2022)

45. J. Zhang, M. Li, H. Wei, Y.J. Su, Z. Yang, Y.F. Zhang, ZnO nanoplate clusters with numerous enlarged catalytic interface exposures via a hydrothermal method for improved and recyclable photocatalytic activity. J. Mater. Sci. Mater. Electron. **29**, 1576–1583 (2018)

46. S. Dey, S. Das, A.K. Kar, Role of precursor dependent nanostructures of ZnO on its optical and photocatalytic activity and influence of FRET between ZnO and methylene blue dye on photocatalysis. Mater. Chem. Phys. **270**, 124872 (2021)

47. R. Rameshbabu, N. Kumar, A. Karthigeyan, B. Neppolian, Visible light photocatalytic activities of $ZnFe_2O_4$/ZnO nanoparticles for the degradation of organic pollutants. Mater. Chem. Phys. **181**, 106–115 (2016)

48. L. Chen, I. Batjikh, J. Hurh, Y.X. Han, Y. Huo, H. Ali, J.F. Li, E.J. Rupa, J.C. Ahn, R. Mathiyalagan, D.C. Yang, Green synthesis of zinc oxide nanoparticles from root extract of *Scutellaria baicalensis* and its photocatalytic degradation activity using methylene blue. Optik **184**, 324–329 (2019)

49. M. Wang, Y.Y. Guo, Z.Q. Zhu, Q. Liu, T.M. Sun, H.H. Cui, Y.F. Tang, Diethanolamine-assisted and morphology controllable synthesis of ZnO with enhanced photocatalytic activities. Mater. Lett. **299**, 130114 (2021)

50. M. Abdelkrim, M. Guezzoul, M. Bedrouni, M. Bouslama, A. Ouerdane, B. Kharroubi, Effect of slight cobalt incorporation on the chemical, structural, morphological, optoelectronic, and photocatalytic properties of ZnO thin film. J. Alloy. Compd. **920**, 165703 (2022)